Article

Molecular Structural Characteristics and 3D Model Reconstruction of Organic Matter in Longmaxi Formation Shale

Jing Liu, Fuhua Shang,* Yanming Zhu,* Shike Li, Guangjun Feng, and Bin Gao

Read Online

ACCESS | Metrics & More | Article Recommendations

ABSTRACT: The establishment of molecular structure modeling is an important means to study the pore characteristics of shale organic matter and is significant for molecular-level simulations of gas storage and diffusion. Using ^{13}C NMR, FTIR, and XPS combined with the split-peak fitting technique, the structural characteristics of the aromatic structure, aliphatic structure, and oxygen functional groups of kerogen from the shale of the Longmaxi Formation, Wuxi County, Chongqing Municipality, were quantitatively characterized. A macromolecular structure model of the kerogen was also constructed by using the 2D macromolecular structure model construction method in combination with elemental analysis experiments. The results showed that the 2D single-molecule structural model of the sample consisted of 2 benzenes, 2 naphthalenes, 1 anthracene, 5 pyrenes, 1 pyridine, and 1 pyrrole. The C skeleton types were 93 protonated arylons, 39 bridged arylons, 6 carboxylons, 5 alkyl-substituted carbons, 2 oxygen-substituted carbons, 4 methylene carbons, and 3 methylons. The established 2D molecular structure formula was $C_{152}H_{82}O_{12}N_2$. The final 3D macromolecular structure model consisted of 14 2D molecular structures (structural formula $C_{2128}H_{1148}O_{168}N_{28}$), with the density set to 1.77 cm^3/g, compressed in a cubic cell with an edge length of 3.05 nm. Finally, the adsorption results showed that the experimental adsorption of CO_2 adsorption was less than the simulated adsorption, completing the validation of the model. The above study provides a method for determining the molecular structure of kerogen in the Longmaxi Formation shale, which can guide the study of the pore structure characteristics of the Longmaxi Formation shale.
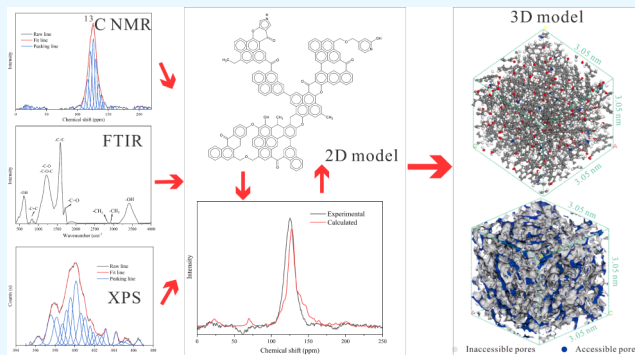
1. INTRODUCTION

Shale gas has become an indispensable and important part of energy and has great potential for development. Although a number of countries have achieved large-scale mass production of shale gas, the actual energy gap is still large. As the world's largest developing country, China's demand for clean energy, such as shale gas, is growing daily under the premise of low-carbon development. The high production and successful extraction of shale gas from the Longmaxi Formation in the Jiao Shi Ba area located in eastern Sichuan demonstrate the great potential of shale gas extraction in China.[1] To ensure the supply of energy, work such as evaluating and researching shale gas has become crucial.

The Longmaxi Formation shale has a high organic matter content and good potential for gasification.[2] Moreover, pores created during the thermal evolution of organic matter provide storage space for shale gas.[3,4] In addition, the study of gas adsorption desorption and diffusion behavior in organic matter nanopores is also important for understanding the effect of organic matter on shale gas storage.[5,6]

The type of organic matter has an important effect on shale gas capacity. The type of organic matter is mainly divided into type I, type II, and type III, and different types of kerogen have different oil- and gas-generating capacities. Among them, type I mainly produces oil, and the source of material is lower algae, and type II produces both oil and gas, and the source of material is marine sediments, and type III mainly produces gas, and the source of material is higher plants.[7,8] In addition to organic matter abundance and type, organic matter maturity is equally important for shale gas generation and reservoirs.[9,10] In thermal evolution, organic matter changes pore structure characteristics at the nanoscale through processes such as hydrocarbon generation.[11−13]

Organic matter pores are important components of shale pores, and previous researchers have performed much research on the effect of organic matter on the pore structure of shale

and organic matter pores.[14−16] Methane and other gases in organic matter species are mainly in two states—adsorbed and free—and adsorbed gas is dominant, accounting for approximately 60% to 80% of the total gas content.[17,18] The process of hydrocarbon production from organic matter may lead to the opening of otherwise closed, independent pores, creating a transportation network for natural gas.[19,20] Current research on shale organic matter has focused mainly on the study of the structure of kerogen itself, which is separated from shale by means of acid washing and other treatments, to obtain kerogen.[21,22]

In recent years, an increasing number of scholars have investigated the molecular structural characteristics of coal and shale organic matter. A variety of microcellular spectroscopy experiments, including ^{13}C NMR, FTIR, XRD, and XPS, have been widely used to obtain structural information about kerogen and quantify the relative proportions of chemical groups, such as carbon skeletons, aliphatic groups, functional groups, heteroatoms, and bonding parameters.[23−26] Moreover, HRTEM can also visualize the quantitative structural parameters of aromatic lamellae to support the molecular structure characterization results.[27] In addition to the above individual experimental analyses, some scholars have established an average molecular 2D structural model for kerogen based on kerogen elemental analysis and molecular structure characterization experimental data.[28,29] With the development of computer technology, several novel means of molecular structure simulation have emerged. Simulation software has been used to further develop traditional 2D structural models into more intuitive 3D structural models.[30,31] The construction and optimization of 2D models and density tests led to 3D structural models of the coal speciation group and shale kerogen molecules.[22,28] In the previous studies, the scientific validity of the molecular structure was mainly verified by comparing the ^{13}C NMR spectra with the simulated spectra, and by comparing the established 2D molecular structure with other molecular structure testing experiments. In this paper, the proportion of various types of structural fragments is calculated directly by using molecular structure testing experiments, and the construction of molecular structure is completed directly, which avoids the phenomenon of unreasonable structural collocation in the modeling process to a certain extent, and at the same time, it can simplify the process of molecular structure establishment.

As the most successful shale gas development area in the Sichuan Basin, many areas within the basin have development potential, and the Chengkou-Wuxi area in the Upper Yangzi region is considered to be the most stable shale development area in the Longmaxi Formation.[32,33] A series of studies have been done on the Longmaxi Formation shales in the Wuxi area of Chongqing Municipality, and the black shales of the Longmaxi Formation in the Wuxi area are characterized by extensive development, large thickness, high abundance of organic matter, high maturity, etc., and are considered to have a good prospect for exploration and development.[34−36]

In this paper, the Longmaxi Formation shale kerogen was used as the research counterpart, and Raman spectroscopy was first utilized to determine the maturity of the samples. ^{13}C NMR, FTIR and XPS were used to obtain the structural fragments of kerogen, and elemental analyses were used to obtain the atomic ratios of each element and to construct 2D and 3D molecular structure models of the Longmaxi Formation shale. Thus, we can understand the pore structure

characteristics of shale organic matter and provide a reference for further research on the characteristics of shale gas reservoirs in the Longmaxi Formation.

2. SAMPLE AND METHODS

2.1. Sample Preparation. The sample is a gray−black organic-rich shale from the Wuxi area in northeastern Chongqing that belongs to the Silurian Longmaxi Formation; it has horizontally developed stratigraphy and contains a large number of penstock fossils. Since the establishment of the molecular structure is mainly based on the organic matter portion of the sample and since shale samples contain a large number of other minerals, the organic matter (kerogen) in the shale samples needs to be purified to obtain structural information. Prior to kerogen extraction, the weathered surface of the samples was removed, the fresh portion of the interior of the samples was retained, and the major minerals in the shale samples were removed using HCl and HF, two solvents that have been shown by previous studies to have a low effect on organic matter.[37] Subsequent removal of heavy metals from the samples using heavy liquid separation methods. No organic solvents were used to remove small molecules of organic matter during the separation process. Therefore, the samples can be better modeled by reducing the average molecular structure of the organic matter.

2.2. Characterization of Chemical Structure Information. *2.2.1. Raman Experiment.* Maturity is an indicator of the ability of shale organic matter to become angry and can reflect the stage at which gas is produced. Raman spectroscopy was used to calculate the maturity of the samples, and previous studies have shown that the maturity of Raman data can be calculated by using the difference in peak displacement between the D peak and the G peak for wavenumbers in the range of 1000−2000 cm^{-1}, where the D peak represents the lattice defects of the C atoms, and the G peak is the in-plane telescopic vibration of the sp^2 hybridization of the C atoms. And maturity are strongly correlated, the calculation formula is as follows:[38]

$$R_O = 0.0537d(G - D) - 11.21 \tag{1}$$

where R_O is the Raman reflectivity and $d(G - D)$ is the peak displacement difference.

2.2.2. Kerogen Structural Fragments. Before constructing the 3D molecular structure of kerogen, it is necessary to obtain information on the structural fragments of kerogen. ^{13}C NMR, XPS, FTIR, and other experiments were utilized to obtain chemical structure information for the kerogen. The chemical structure information on each experiment is a prerequisite for the establishment of a 2D kerogen molecular structure. ^{13}C NMR is the basis of the whole model construction, reflecting the carbon spectrum information in the sample. The instrument used was a high-resolution Bruker advance III 600 MHz spectrometer. The instrument used for the XPS experiments was an ESCALAB250 Xi surface analysis system. The instrument used for the FTIR experiments was a Vertex 80v instrument and a Fourier transform infrared spectroscopy instrument.

2.3. Methods for Determining the Structure of Kerogen. The establishment of a 2D molecular structure needs to be accomplished by roughly calculating the molecular formula of the single-molecule structure based on the atomic ratios obtained from the elemental analyses combined with the percentage of information on the various types of chemical
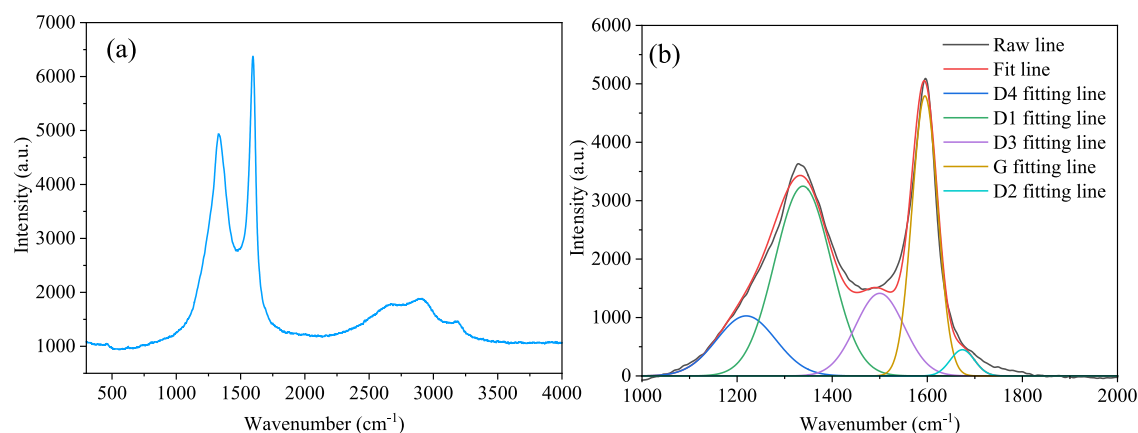
Figure 1. Raman spectrum of the sample (a, original atlas; b, fit spectrogram).

structures. ACD/C NMR Predictors software was used to construct the 2D kerogen macromolecular structure and calculate its ^{13}C NMR profile information. The computational and experimental ^{13}C NMR profiles were compared, and if the data from the two profiles are consistent, the established 2D molecular structure model is reasonable. If the two have large differences, the models need to be reconstructed and compared again until a reasonable 2D molecular structure model is obtained.

After the 2D molecular structure was built, the 2D structure file was imported into Materials Studio (Accelrys) software, and the 2D molecular structure was geometrically optimized and annealed to select the lowest energy model before building the 3D model. Since the edge length of 3D structural models is generally above 3 nm,[39] to realize this requirement, 14 or more 2D single molecules are usually selected to form a 3D molecular structure model, and the density parameters of the structure are also set based on the preliminary kerogen density test data to establish the 3D molecular structure. Structural optimization and annealing operations are again performed on the basis of the established 3D structure. CO_2 (diameter = 0.33 nm) was used as a molecular probe to measure the pores of the 3D structural model, and the results were compared with those of CO_2 adsorption experiments to construct a suitable 3D molecular structure model.

3. RESULTS AND DISCUSSION

3.1. Sample Maturity. Vitrinite reflectance is a commonly used method for measuring the maturity of sedimentary rocks.[40,41] Moreover, the content of vitrinite in shale is very low or even nonexistent.[37,42] Previous studies have shown that Raman data can be used to calculate sample maturity.[38,42] Figure 1 shows the Raman spectrum of the shale sample. Figure 1a shows the Raman spectrum of the original sample, where the two peaks at 1000−2000 cm^{-1} are the D peak and the G peak. By performing peak fitting on the curve in Figure 1a at 1000−2000 cm^{-1}, the fitted D peak wavenumber was 1338.5 cm^{-1}, and the G peak wavenumber was 1595 cm^{-1}. The maturity of the tested samples was calculated as R_O = 2.56%, which is an overmature stage. To verify the accuracy of the calculation results, the former test data were used for verification (Figure 2), and the results showed that the greater the reflectivity of the specular group was, the greater the difference in peak displacement was.[43,44] The calculated peak displacement difference of 256.5 cm^{-1} corresponds to a maturity of approximately 2.5% in Figure 2, which is consistent
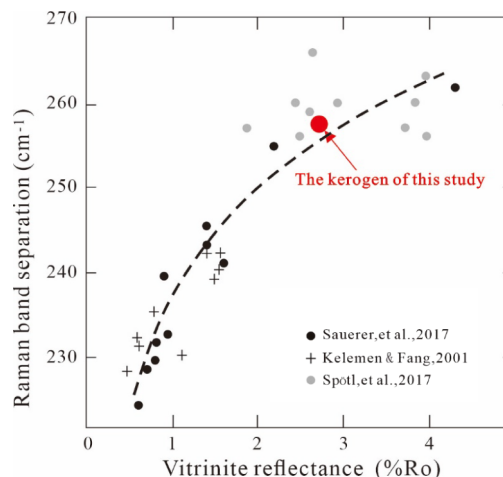

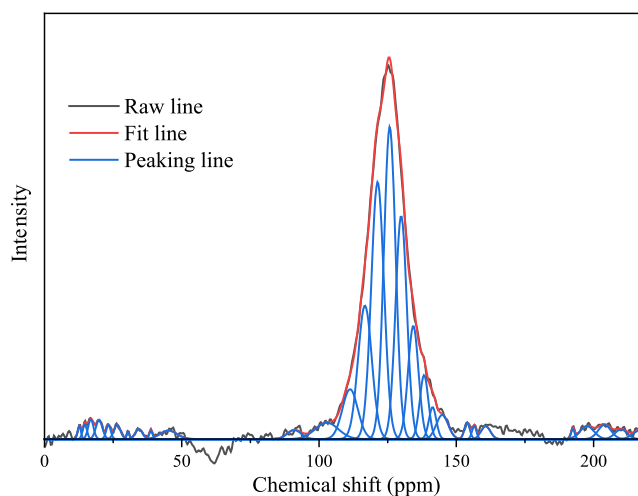**Figure 2.** Correlation plot of maturity and peak difference.[44]

Figure 3. ^{13}C NMR fitting pattern.

with the calculated results; therefore, the calculated maturity is credible.

3.2. ^{13}C NMR Data. ^{13}C NMR can reveal the detailed chemical structure of the samples. Figure 3 shows the ^{13}C NMR pattern of the selected sample. The plots show that the chemical shifts have very distinct peaks in the range of 90−165 ppm, indicating that the C in the samples is mainly aromatic. There are also some small peaks in the range of 0−50 ppm and

Table 1. ^{13}C NMR Structural Parameters of the Sample

| integration region	structure parameters	chemical shift(ppm)	ratio(%)
carboxyl, carbonyl carbon	f_a^c	165−240	3.88
phenolic	f_a^P	150−165	1.62
alkylated aromatic	f_a^S	137−150	3.18
aromatic bridgehead	f_a^B	129−137	25.82
protonated and aromatic	f_a^H	100−129	60.89
bonded to oxygen	f_{al}^O	50−90	0.00
CH or CH_2	f_{al}^H	22−90-(50−60)	2.57
CH_3 or nonprotonated	f_{al}^*	0−22 and 50−60	2.04
nonprotonated and aromatic	f_a^N	P+S+B	30.62
in an aromatic	f_a'	N+H, 90−165	91.51
total aromatic carbon	f_a	90−240	95.39
total aliphatic carbon	f_{al}	0−90	4.61
aromatic bridgehead	X_{BP}		0.39
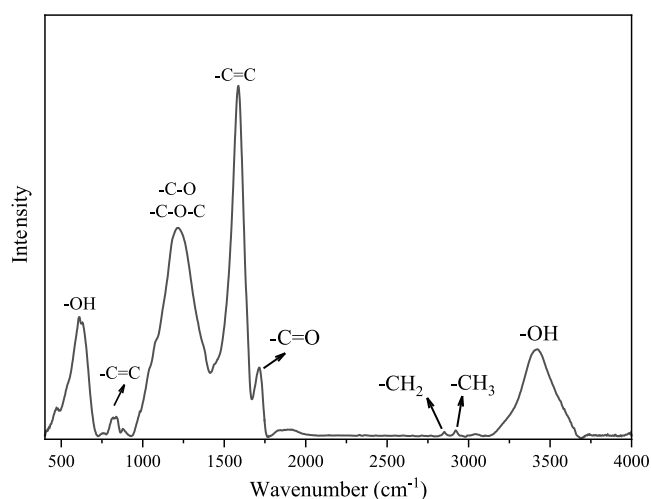
Figure 4. FTIR profile of the Longmaxi shale kerogen.

near 200 pm, but their peak intensities are relatively low, indicating that there are a certain number of aliphatic carbon and carboxy-carbonyl functional groups in the samples. The structural characteristics of the carbon skeleton can be obtained by fitting the split peaks to the ^{13}C NMR pattern, and the fitted computationally fitted pattern is consistent with the experimental pattern, indicating that the split peak results

Table 2. Absorption Peaks of Oxygen Functional Groups Assigned to the FTIR Spectra

peak	attribution	center	width	area	area ratio(%)
1	alkyl ether C−O	1023.282	83.148	1.395	2.62
2	aryl ether C−O	1085.818	98.546	3.688	6.94
3	phenol OH	1172.690	109.809	8.282	15.58
4	phenol OH	1248.290	113.766	9.695	18.24
5	phenol OH	1322.666	98.748	3.938	7.41
6	CH_3	1381.358	79.949	2.241	4.21
7	CH_3;CH_2 asymmetric deformation vibration	1441.411	57.358	1.316	2.48
8	aromatic C=C	1490.972	84.993	2.101	3.95
9	aromatic C=C	1536.668	83.989	5.393	10.14
10	aromatic C=C	1587.744	62.271	10.733	20.19
11	conjugated C=O vibration	1632.124	43.310	2.030	3.82
12	C=O stretching vibration	1684.800	48.247	0.888	1.67
13	C=O stretching vibratio	1718.524	43.079	1.464	2.75

Table 3. Absorption Peaks of Aliphatic Structures Assigned to the FTIR Spectra

peak	attribution	center	width	area	area ratio(%)
1	sym. R_2CH_2	2827.978	17.305	0.008	4.72
2	sym. R_2CH_2	2850.549	20.764	0.048	27.76
3	sym. RCH_3	2871.616	23.311	0.013	7.64
4	R_3CH	2899.667	24.511	0.015	8.64
5	asym. R_2CH_2	2921.851	22.899	0.075	43.15
6	asym. RCH_3	2950.903	27.272	0.014	8.09

are more reasonable (Figure 3). Because different peak displacements represent different attributions of C and because the ratio of different peak areas to the total area represents the percentage of C in the region, the attribution and percentage of each type of C can be obtained via calculation (Table 1). The ratio of aromatic bridge carbon to periphery carbon (X_{BP}) was further calculated based on the results for each type of C.[45] X_{BP} can be used for subsequent calculations of aromatic carbon distributions,[46] and the calculation formula is as follows:
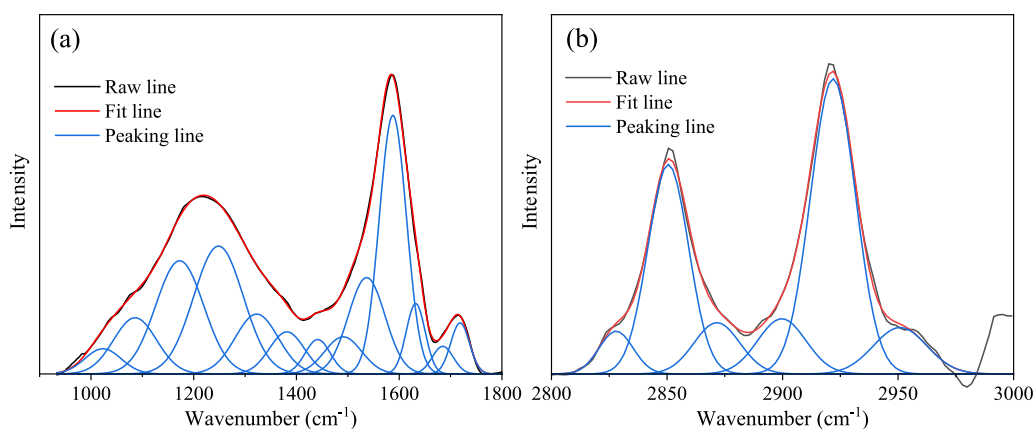
$$X_{BP} = f_a^B / f_a^N \tag{2}$$

Figure 5. Curve-fitted FTIR spectra of the Longmaxi shale kerogen (a, oxygen functional group; b, aliphatic structures).
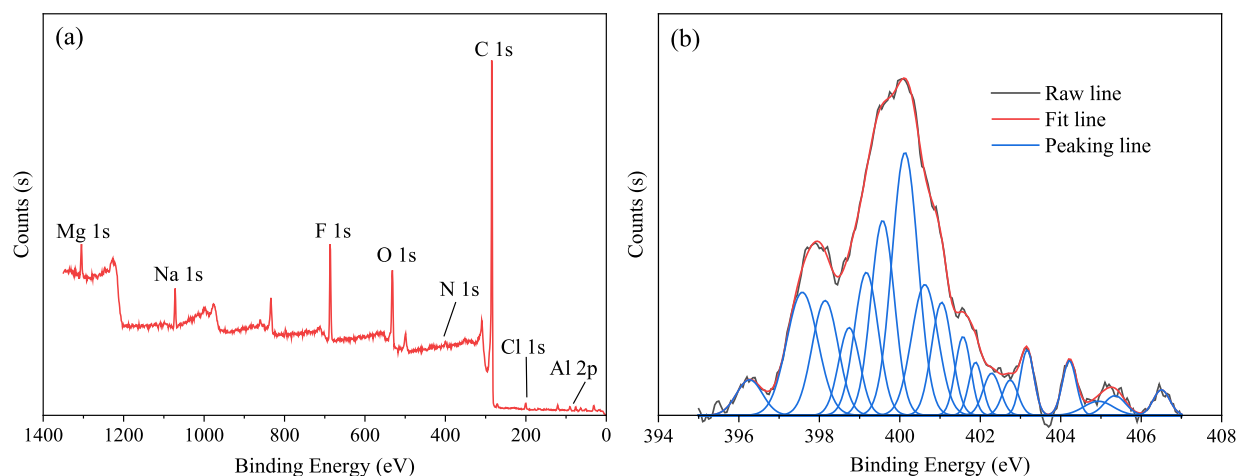
Figure 6. XPS characteristic spectra of the Longmaxi shale kerogen (a, wide scan; b, N 1s scan).

Table 4. Percentage of Kerogen in the Longmaxi Formation Shale (XPS)

element	peak BE	fwhm (eV)	area	area ratio (%)
C 1s	284.62	2.82	901501.72	75.5
F 1s	686.47	3.41	295242.49	7.52
O 1s	531.96	4.19	289890.17	9.56
Mg 1s	1304.94	3.3	91417.03	1.42
Na 1s	1071.97	3.31	111064.35	1.59
Cl 2p	200.55	3.63	24825.43	0.73
N 1s	399.72	4.45	34283.46	1.81
Al 2p	75.99	3.11	13206.69	1.81
S 2p	163.22	0.63	108.53	0.04

Table 5. Peak-Fitting Results of the N 1s Spectrum

peak BE	area	area ratio (%)	attribution
396.26−397.58	184.95	13	pyridine
398.14−399.57	496.60	35	pyrrole
400.13−403.16	646.08	46	protonated pyridine
404.22−406.50	77.95	6	N-pyridine oxide

3.3. FTIR Data. Figure 4 shows the FTIR pattern of kerogen for the selected samples. The position and relative intensity of the absorption peaks can determine the type and percentage of chemical groups in kerogen. Different bands represent different types of chemical groups, and each chemical group has its own specific range of bands. Chemical group information can be determined based on the fluctuation characteristics of the FTIR pattern. Kogen has mainly aromatic structures, aliphatic side chains, and oxygenated functional groups (Figure 4). Here, the oxygen functional groups and aliphatic structures in kerogen were quantified using FTIR (Figure 5).

Figure 5a shows the results of the peak splitting of the oxygen functional groups of the samples. Based on the classification methods of relevant scholars, the groups represented by each fitted peak were categorized. Oxygen functional groups generally include methoxy, carboxyl, hydroxyl and etheroxyl groups. In the Longmaxi Formation shale kerogen in this study, the oxygen functional groups mainly consisted of phenolic hydroxyl groups, followed by etheroxyl groups, and the contents of other oxygen functional groups were relatively low (Table 2). Figure 5b shows the fitting results for the aliphatic structure, which were fitted using 5−6 peaks, and the fitting parameters were integrated into Table 3 based on the fitting profile. The results showed that the highest percentage of methylene was found in the samples, which was as high as 75.63%, while 15.73 and 8.64% were methyl and hypomethyl, respectively.

3.4. XPS Data. XPS experiments are also important for characterizing the chemical structure of kerogen.[47,48] Figure 6a shows the XPS wide-scan spectrum of the Longmaxi Formation shale kerogen, which reveals that the content of C atoms is in the absolute position in the spectrum, and the relative content of each element can be obtained after the calculation of the spectrum (Table 4). The results showed that the samples were dominated by C, O, and F atoms, whereas in general, kerogen does not contain F atoms. This difference may be due to the residual hydrofluoric acid used in the extraction of kerogen. In addition, the plots showed that the samples contained metal elements such as Mg and Zn, indicating that some metal residues were still present during the purification of the kerogen. The attribution of the C skeleton and oxygen functional groups in kerogen has been investigated previously using ^{13}C NMR and FTIR, and it is sufficient to analyze the N and S in kerogen using XPS. Since the content of S in the sample is very low, it has no effect on the establishment of the molecular structure of kerogen, so the calculation of the attribution of N can be used to establish the molecular structure of kerogen. Figure 6b shows the fitted spectra of N atoms, which were first smoothed, and the fitted peaks were subsequently used to calculate the attribution of N atoms because the original spectra were too cluttered for the fitting process (Table 5). The results showed that the N atoms

Table 6. Ultimate Analysis Results and Atom Ratio After Allocation

ultimate analysis (%)					atomic ratio			
C'_{daf}	H'_{daf}	O'_{daf}	N'_{daf}	$S_{t,d}$	H'/C'	O'/C'	N'/C'	S'/C'
83.05	2.44	12.62	1.74	0	0.3530	0.1140	0.0179	0

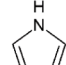**Table 7. Types and Amounts of Aromatic Structural Units Were Assumed**
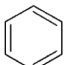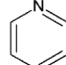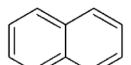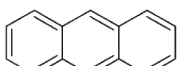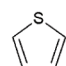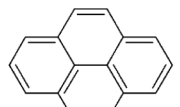
Structure	Name	number·	Structure	Name	number·
	Benzene	a		Pyridine	1
	Napthalene	b		Pyrrole	1
	Anthracene	c		Thiophene	0
	Pyrene	d			

Table 8. Table of 2D Molecular Structure Parameters of Test Sample

	name	number
aromatic structural unit	benzene	2
	naphthalene	2
	anthracene	1
	pyrene	5
	pyridine	1
	pyrrole	1
aromatic carbon	protonated aromatic carbon	93
	bridged aromatic carbon	39
	carboxylic carbon	6
	alkyl-substituted carbon	5
	oxygen-substituted carbon	2
aliphatic carbon	methylene carbon	4
	methyl carbon	3

in kerogen were mainly protonated pyridine and pyrrole, accounting for 46% and 35%, respectively.

3.5. Molecular Model Construction. *3.5.1. 2D Molecular Model.* The structural fragments of the sample molecule have been briefly analyzed previously, and the establishment of a 2D structure can be accomplished based on the structural fragments. Before the establishment of the molecular structure, the number of individual atoms in a single 2D molecular structure model is determined. The determination of the molecular structure relies mainly on elemental analysis experiments. Due to the low content of S, S can be ignored when the structure is built, but the content of S needs to be redistributed. The distribution scheme needs to be based on the atomic ratios of the four atoms, C, H, O, and N, and the specific distribution method is as follows:

$$X'_{daf} = X_{daf} + S_{daf}*X_{daf}/(C_{daf} + H_{daf} + O_{daf} + N_{daf}) \tag{3}$$

where X'_{daf} is the elemental content of C, H, O, and N atoms after repartitioning and X_{daf} is the experimental content of C, H, O, and N atoms.

The percentage of each element in the kerogen after redistribution can be obtained from eq 2 (Table 6), and the ratio of the number of different elements to the number of C atoms can be obtained from eq 4.

$$X'/C' = X'_{daf}*M_C/(C'_{daf}*M_X) \tag{4}$$

where X' is the number of atoms, which can be H, O, N, or S; C' is the number of C atoms; M_C is the relative molecular mass of C; and M_X is the relative molecular mass of different atoms.

Thus, a molecular structural formula can be obtained for a kerogen structure based on C atoms and containing only one variable. Setting the number of C atoms to n, the molecular formula is available as $C_nH_{0.353n}O_{0.114n}N_{0.0179n}$.

Based on the results of the previous ^{13}C NMR analyses, the C in kerogen was classified. Based on the obtained structural parameters of the 12 C skeletons, the average value of X_{BP} for characterizing the degree of aryl ring condensation was calculated. The attribution and number of C atoms in the aromatic structural units of the kerogen structure can be determined from X_{BP}. The results showed that the X_{BP} of the selected sample's kerogen was 0.39, indicating that the aromatic structure in this sample was mainly dominated by anthracycline and pyrene, supplemented by other types of aromatic structures. The number of C atoms in the kerogen sample can be calculated using eq 5. The molecular formula of the macromolecular structure of kerogen was calculated to be $C_nH_{0.353n}O_{0.114n}N_{0.0179n}$, and previous studies have indicated that the relative molecular weight of organic matter is generally between 2000 and 3000.[49] The atomic number of C atoms in this sample was calculated to be 152, resulting in a molecular structure formula of $C_{152}H_{54}O_{17}N_2$, with subsequent adjustments based on other atomic contents.

The above experiments were completed to determine the number of C atoms in the kerogen, and the initial molecular structural formula was obtained. The optimization of the molecular structural formula needs to be continued and completed based on the number of O atoms and N and S atoms. The structural information on the oxygen functional groups obtained using FTIR showed that the samples contained four oxygen functional groups, namely, alkyl ether, aryl ether, phenolic hydroxyl group and carbonyl group. Combined with the results of ^{13}C NMR analysis, it can be concluded that the ratio of these four types of oxygen functional groups is 1:2:1:3, and the content of O atoms should be 12, so that the above oxygen functional groups are 2, 4, 2 and 6, respectively. In addition, according to the XPS experiments, the N atoms in the samples were present as pyridine nitrogen and protonated pyridine nitrogen, which can be combined here, and pyrrole nitrogen also occupied a considerable proportion of the sample. The results show that the ratio of the two is approximately 3:2; to ensure an integer
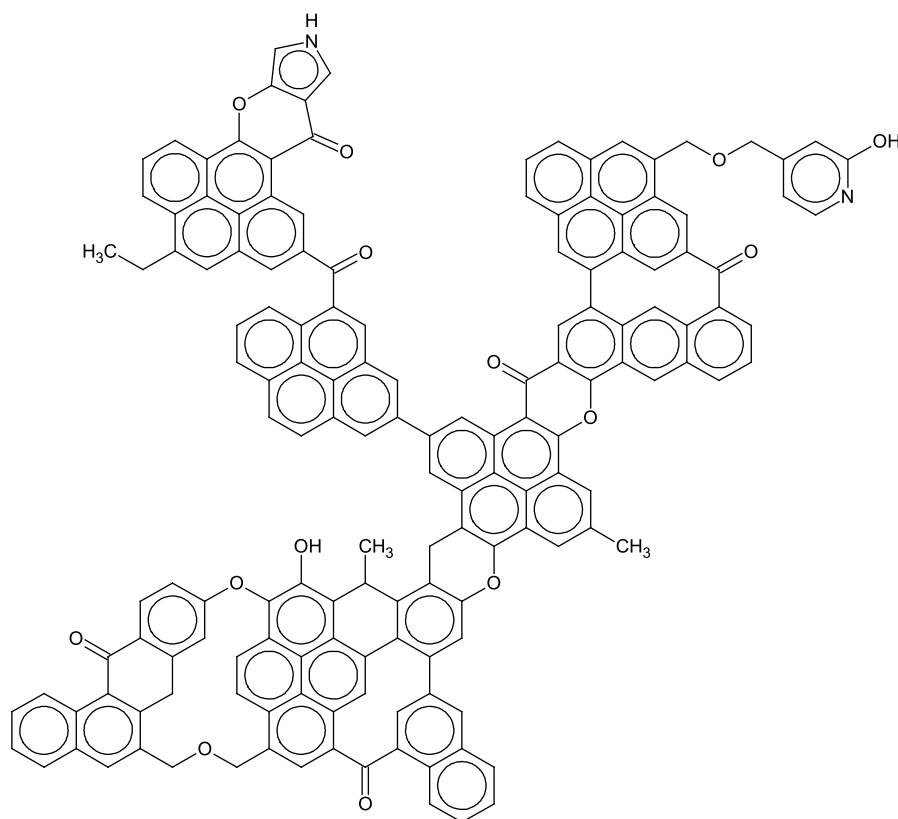
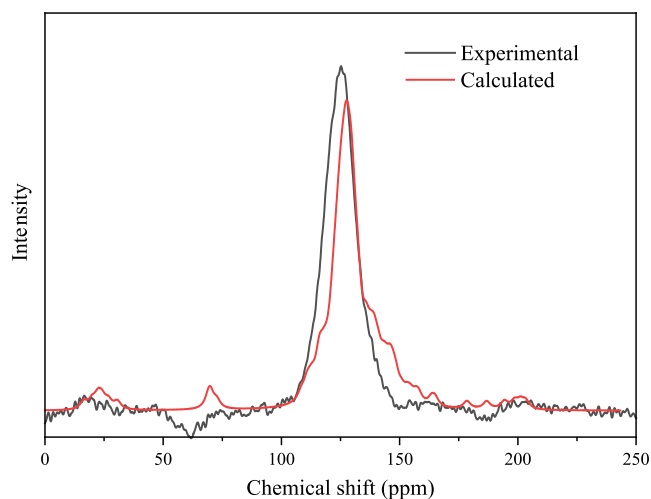**Figure 7.** 2D monomolecular structure of the Longmaxi shale kerogen.

Figure 8. Comparison of the ^{13}C NMR simulated spectra with the experimental.

Figure 9. 3D chemical structure of the Longmaxi shale kerogen.

distribution of N atoms, the two N atoms in the formula can be evenly distributed to pyridine and pyrrole. Due to the negligible presence of S atoms in the element, the allocation of S atoms will not be carried out here. The molecular formula of the established kerogen structure model is $C_{152}H_{82}O_{12}N_2$, with a relative molecular weight of 2160.28, which is consistent with the expected results.

The number of C, O, and N atoms was determined, and the types and quantities of oxygen functional groups and N functional groups were calculated. By further determining the aromatic structure based on the parameter distribution in Table 7, the molecu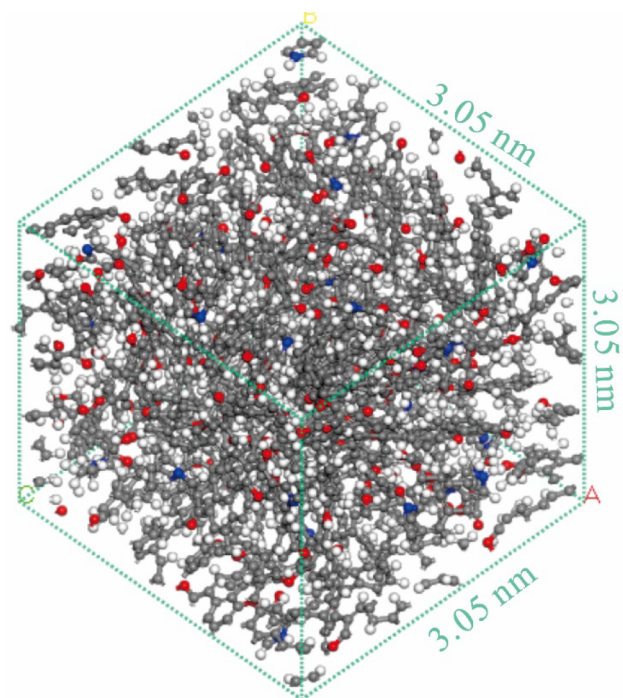lar structure can be established. The number of aromatic structures can be calculated using eqs 5 and 6. Due to the presence of numerous variables, the results also exhibit multiple solutions. Therefore, it is necessary to assign values to the aromatic structure first and select the optimal solution.
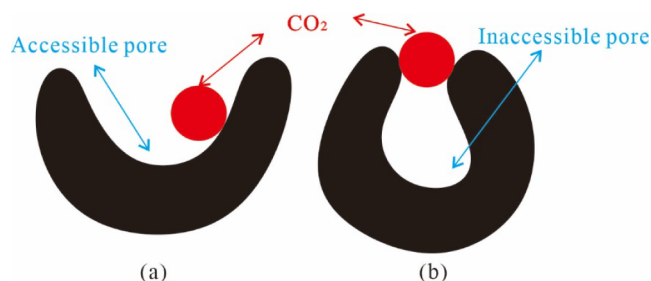
Figure 10. Pore types detected by molecular probes (a, accessible pore; b, inaccessible).
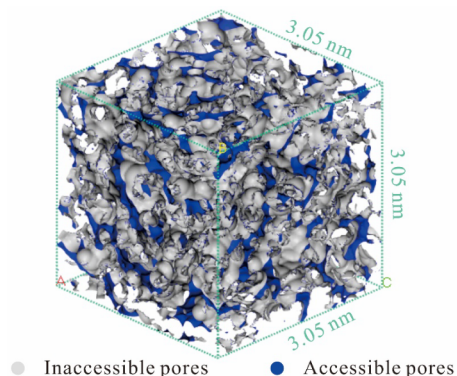

○ Inaccessible pores   ● Accessible pores

Figure 11. Pore type diagram of the 3D kerogen molecular structure.

$$(2b + 4c + 6d)/(6a + 8b + 10c + 10d + 9) = X_{BP} \tag{5}$$

$$6a + 10b + 14c + 16d + 9 = F_a \tag{6}$$

where F_a represents the number of aromatic C atoms.

Table 8 shows the structural parameters of the final single molecule. The aromatic structure contains 2 benzenes, 2 naphthalenes, 1 anthracene, and 5 pyrenes in the aromatic structure. One pyridine and one pyrrole are present simultaneously. In addition, the C-skeleton type comprises 145 aromatic carbons (93 protonated aromatic carbons, 39 bridged aromatic carbons, 6 carboxylic carbons, 5 alkyl-substituted carbons, and 2 oxygen-substituted carbons) and 7 aliphatic carbons (4 methylene carbons and 3 methyl carbons).

Based on the proportion of each functional group, a 2D model of the structure of kerogen was obtained using ChemSketch and g NMR software (Figure 7). The predicted model of kerogen was compared with the experimental values, and the structural model was adjusted again when the two did not match until the simulated ^{13}C NMR spectrum results were basically consistent with the experimental spectrum (Figure 8).

3.5.2. 3D Molecular Model. The obtained 2D molecular structure model of kerogen and the true density of kerogen obtained from experimental testing can be used to establish a 3D molecular structure model in Materials Studio software. Before establishing the 3D molecular structure, the obtained 2D structural model was first imported into Materials Studio software and optimized through annealing to obtain suitable structural fragments. This model places 14 optimized 2D kerogen molecular models into a cubic cell box with a side length of 3.05 nm using the AC module. and the lowest-energy model was selected by the Compass II force field calculation van der Waals Force. Since the density test result of the sample casein was 1.77 g/cm^{-3}, the 3D molecular structure model

with different porosity values was obtained by setting the density parameter to 1.77 g/cm^{-3} in the software.

The porosity of each output configuration was calculated based on the pore testing tool in the software, and the pore testing tool was used to calculate the porosity of each configuration. CO_2 adsorption experiments at a temperature of 298 K showed a maximum adsorption of 0.06 cm^3/g, while the simulation results at a temperature of 298 K showed an adsorption of 0.08 cm^3/g. Since the kerogen in the test sample contains a certain amount of minerals such as metals and since the 3D structural model includes pure organic matter, the experimental adsorption amount is slightly lower than the simulated adsorption amount, which is a normal phenomenon; moreover, the simulation model is reasonable, and the 3D model of the sample is shown in Figure 9.

Due to the difference in pore connectivity, part of the pores can be directly probed, and the other part of the pores cannot be directly reached (Figure 10). In this paper, by using CO_2 as a probe, pores with pore sizes larger than the molecular radius of CO_2 can be detected. The pores that can be directly probed become accessible pores; otherwise, they are inaccessible pores. Figure 11 shows a pore type diagram of the 3D kerogen molecular structure, which reveals that both accessible and inaccessible pores are equally present in the kerogen structure. The results showed that the amount of CO_2 adsorbed should be slightly different than the actual amount adsorbed. Therefore, adsorption experiments cannot reveal the adsorption capacity of kerogen completely, which is also a disadvantage of adsorption experiments.

The molecular structure of kerogen is not homogeneous but consists of various types of molecular structures of different sizes and with a variety of connections. The above molecular structure model is based on the 2D average molecular structure, which is an average molecular structure model. Previous researchers have also done some studies on the molecular structure model of kerogen, and some scholars have constructed the molecular structure of kerogen from Longmaxi Formation shale in Changning area.[50] The results show that the model established in this study has some common points and some differences compared with it, and the differences are mainly the higher aromaticity of this model and the structure of cyclohexane and other structures were not used, which may be due to the fact that the soluble organic matter was retained in this experiment, so that the average structural model of the samples was different from the structure of the eliminated soluble organic matter. Although this model and other models cannot fully represent the macromolecular structure of kerogen, they are the closest to the original structure. Although this model does not fully represent the macromolecular structure of kerogen, it is the closest model to the original structure. The molecular structure characteristics will be further investigated, and the structure will be improved in subsequent studies.

4. SUMMARY AND CONCLUSIONS

(1) The maturity of the Longmaxi Formation shale sample in this experiment is R_O = 2.56%, which belongs to the overmature stage; the aromatic structures in the sample are mainly dominated by anthracenes and pyrenes; the oxygen functional groups are mainly dominated by phenolic hydroxyl groups, followed by ether oxygens; the aliphatic structures have the highest proportion of submethyl groups; and the

proportions of methyl groups and hypomethyl groups are relatively small.

(2) In this paper, the aromatic structures in the 2D single-molecule structure of kerogen from the Longmaxi Formation shale include 2 benzenes, 2 naphthalenes, 1 anthracene and 5 pyrenes. One pyridine and 1 pyrrole are also present. In addition, the C-skeleton type comprises 145 aromatic carbons (93 protonated aryl carbons, 39 bridged aryl carbons, 6 carboxylic carbons, 5 alkyl-substituted carbons, and 2 oxygen-substituted carbons) and 7 aliphatic carbons (4 methylene carbons and 3 methyl carbons). The 3D unimolecular structure consists of 14 2D unimolecular structures with a cell size of 3.05 nm and a density of 1.77 g/cm^{-3}.

(3) The existence of accessible and inaccessible pores in the kerogen structure indicates that the CO_2 adsorption capacity should be lower than the actual adsorption capacity, and traditional CO_2 adsorption experiments cannot be used to determine the pore structure of kerogen; moreover, new means of solving this problem need to be further investigated.

■ AUTHOR INFORMATION

Corresponding Authors

Yanming Zhu − Key Laboratory of Coalbed Methane Resources and Reservoir Formation Process of the Ministry of Education, China University of Mining and Technology, Xuzhou 221116, China; School of Resources and Geoscience, China University of Mining and Technology, Xuzhou 221116, China; orcid.org/0000-0001-7355-4512; Email: fhshangcumt@163.com

Fuhua Shang − Inner Mongolia Engineering Research Center of Geological Technology and Geotechnical Engineering, Inner Mongolia University of Technology, Hohhot 010051, China; orcid.org/0000-0003-2134-9183; Email: ymzhucumt@126.com

Authors

Jing Liu − School of Emergency Management and Safety Engineering, North China University of Science and Technology, Tangshan 063210, China; orcid.org/0009-0007-1683-6573

Shike Li − School of Emergency Management and Safety Engineering, North China University of Science and Technology, Tangshan 063210, China

Guangjun Feng − Key Laboratory of Coalbed Methane Resources and Reservoir Formation Process of the Ministry of Education, China University of Mining and Technology, Xuzhou 221116, China; School of Resources and Geoscience, China University of Mining and Technology, Xuzhou 221116, China; orcid.org/0000-0002-7084-0836

Bin Gao − Key Laboratory of Coalbed Methane Resources and Reservoir Formation Process of the Ministry of Education, China University of Mining and Technology, Xuzhou 221116, China; School of Resources and Geoscience, China University of Mining and Technology, Xuzhou 221116, China

Complete contact information is available at:
https://pubs.acs.org/10.1021/acsomega.4c00424

Notes

The authors declare no competing financial interest.

J.L. contributed to conceptualization, methodology, writing, and editing. Y.Z. and F.S. contributed to conceptualization, methodology, and funding acquisition. S.L., G.F. and B.G. conducted experiments and contributed to data curation.

■ ACKNOWLEDGMENTS

■ REFERENCES

(1) Guo, T.; Zhang, H. Formation and enrichment mode of Jiaoshiba shale gas field, Sichuan Basin. Pet. Explor. Dev. 2014, 41 (1), 31−40.

(2) Gai, S.; Liu, H.; He, S.; Mo, S.; Chen, S.; Liu, R.; Huang, X.; Tian, J.; Lv, X.; Wu, D.; He, J.; Gu, J. Shale reservoir characteristics and exploration potential in the target: A case study in the Longmaxi Formation from the southern Sichuan Basin of China. J. Nat. Gas Sci. Eng. 2016, 31, 86−97.

(3) Sun, H.; Zhao, H.; Qi, N.; Li, Y. Molecular Insights into the Enhanced Shale Gas Recovery by Carbon Dioxide in Kerogen Slit Nanopores. J. Phys. Chem. C 2017, 121 (18), 10233−10241.

(4) Miao, Y.; Li, X.; Lee, J.; Zhou, Y.; Liu, S.; Chang, Y.; Wang, S. Characterization of hydrocarbon/pores generation and methane adsorption in shale organic matter. Pet. Sci. Technol. 2018, 36 (15), 1187−1193.

(5) Wang, W.; Yao, J.; Sun, H.; Song, W. Influence of gas transport mechanisms on the productivity of multi-stage fractured horizontal wells in shale gas reservoirs. Pet. Sci. 2015, 12 (4), 664−673.

(6) Hu, B.; Wang, J. G. A lattice Boltzmann simulation on the gas flow in fractal organic matter of shale gas reservoirs. J. Pet. Sci. Eng. 2022, 210, 110048.

(7) Donadelli, J. A.; Cánneva, A.; Erra, G.; Calvo, A. XPS direct analysis on shale rocks: Correlation with kerogen type and maturity. Fuel 2019, 257, 116004.

(8) Li, M.; Tan, X.; Wang, G.; Li, Y.; Xu, Q.; Zheng, J.; Yang, Y.; Bai, X.; Ji, Y. Differences of Organic Matter Types of High Maturity Marine Organic-Rich Shale from Wufeng-Longmaxi Formation: Implication for Shale Gas "Sweet Spots" Prediction. Energy Explor. Exploit. 2023, 41 (4), 1325−1343.

(9) Curtis, M. E.; Cardott, B. J.; Sondergeld, C. H.; Rai, C. S. Development of organic porosity in the Woodford Shale with increasing thermal maturity. Int. J. Coal Geol. 2012, 103, 26−31.

(10) Hou, L.; Ma, W.; Luo, X.; Liu, J. Characteristics and quantitative models for hydrocarbon generation-retention-production of shale under ICP conditions: Example from the Chang 7 member in the Ordos Basin. Fuel 2020, 279, 118497.

(11) Tang, X.; Jiang, Z.; Jiang, S.; Wang, P.; Xiang, C. Effect of Organic Matter and Maturity on Pore Size Distribution and Gas Storage Capacity in High-Mature to Post-Mature Shales. Energy Fuels 2016, 30 (11), 8985−8996.

(12) Xu, H.; Zhou, W.; Zhang, R.; Liu, S.; Zhou, Q. Character-izations of pore, mineral and petrographic properties of marine shale using multiple techniques and their implications on gas storage capability for Sichuan Longmaxi gas shale field in China. Fuel 2019, 241, 360−371.

(13) Liu, J.; Zhu, Y.; Shang, F.; Feng, G.; Liu, Y.; Gao, B.; Li, S.; Kuang, F. Pore System Diversity and Control Factors of High-Overmature Shale—Taking the Lujiaping and Longmaxi Formation Shales as an Example. Energy Fuels 2023, 37 (13), 9047−9065.

(14) Alstadt, K. N.; Katti, D. R.; Katti, K. S. An in situ FTIR step-scan photoacoustic investigation of kerogen and minerals in oil shale. Spectrochim. Acta, Part A 2012, 89, 105−113.

(15) Gai, H.; Tian, H.; Xiao, X. Late gas generation potential for different types of shale source rocks: Implications from pyrolysis experiments. Int. J. Coal Geol. 2018, 193, 16−29.

(16) Agrawal, V.; Sharma, S. Are we modeling the properties of unconventional shales correctly? *Fuel* **2020**, *267*, 117316.

(17) Curtis, J. B. Fractured shale-gas systems. *AAPG Bull.* **2002**, *86*, 1921−1938.

(18) Wu, K.; Chen, Z.; Li, X.; Dong, X. Methane storage in nanoporous material at supercritical temperature over a wide range of pressures. *Sci. Rep.* **2016**, *6* (1), 33461.

(19) Zhang, R.; Liu, S.; Bahadur, J.; Elsworth, D.; Melnichenko, Y.; He, L.; Wang, Y. Estimation and modeling of coal pore accessibility using small angle neutron scattering. *Fuel* **2015**, *161*, 323−332.

(20) Collell, J.; Galliero, G.; Vermorel, R.; Ungerer, P.; Yiannourakou, M.; Montel, F.; Pujol, M. Transport of Multi-component Hydrocarbon Mixtures in Shale Organic Matter by Molecular Simulations. *J. Phys. Chem. C* **2015**, *119* (39), 22587−22595.

(21) Vandenbroucke, M.; Largeau, C. Kerogen origin, evolution and structure. *Org. Geochem.* **2007**, *38* (5), 719−833.

(22) Liu, Y.; Liu, S.; Zhang, R.; Zhang, Y. The molecular model of Marcellus shale kerogen: Experimental characterization and structure reconstruction. *Int. J. Coal Geol.* **2021**, *246*, 103833.

(23) Vieira, M. A.; Gonçalves, G. R.; Cipriano, D. F.; Schettino, M. A.; Silva Filho, E. A.; Cunha, A. G.; Emmerich, F. G.; Freitas, J. C. C. Synthesis of graphite oxide from milled graphite studied by solid-state 13C nuclear magnetic resonance. *Carbon* **2016**, *98*, 496−503.

(24) Faisal, H. M. N.; Katti, K. S.; Katti, D. R. An insight into quartz mineral interactions with kerogen in Green River oil shale. *Int. J. Coal Geol.* **2021**, *238*, 103729.

(25) Fan, C.; Yan, J.; Huang, Y.; Han, X.; Jiang, X. XRD and TG-FTIR study of the effect of mineral matrix on the pyrolysis and combustion of organic matter in shale char. *Fuel* **2015**, *139*, 502−510.

(26) Wang, Q.; Hou, Y.; Wu, W.; Yu, Z.; Ren, S.; Liu, Q.; Liu, Z. A study on the structure of Yilan oil shale kerogen based on its alkali-oxygen oxidation yields of benzene carboxylic acids, 13C NMR and XPS. *Fuel Process. Technol.* **2017**, *166*, 30−40.

(27) Shang, F.; Tang, X.; Hu, Q.; Wang, Y.; Meng, X.; Zhu, Y. Chemical Structure Transformations in Kerogen from Longmaxi Shales in Response to Tectonic Stress as Investigated by HRTEM, FTIR, and13 C NMR. *Energy Fuels* **2021**, *35* (23), 19496−19506.

(28) Ungerer, P.; Collell, J.; Yiannourakou, M. Molecular Modeling of the Volumetric and Thermodynamic Properties of Kerogen: Influence of Organic Type and Maturity. *Energy Fuels* **2015**, *29* (1), 91−105.

(29) Wang, T.; Tian, S.; Li, G.; Zhang, L.; Sheng, M.; Ren, W. Molecular simulation of gas adsorption in shale nanopores: A critical review. *Renewable Sustainable Energy Rev.* **2021**, *149*, 111391.

(30) Tong, J.; Jiang, X.; Han, X.; Wang, X. Evaluation of the macromolecular structure of Huadian oil shale kerogen using molecular modeling. *Fuel* **2016**, *181*, 330−339.

(31) Guan, X.; Liu, Y.; Wang, D.; Wang, Q.; Chi, M.; Liu, S.; Liu, C. Three-Dimensional Structure of a Huadian Oil Shale Kerogen Model: An Experimental and Theoretical Study. *Energy Fuels* **2015**, *29* (7), 4122−4136.

(32) Chen, Q.; Zhang, J.; Tang, X.; Li, W.; Li, Z. Relationship between pore type and pore size of marine shale: An example from the Sinian−Cambrian formation, upper Yangtze region, South China. *Int. J. Coal Geol.* **2016**, *158*, 13−28.

(33) Xiao, B.; Xiong, L.; Zhao, Z.; Fu, X. Sedimentary tectonic pattern of Wufeng and Longmaxi Formations in the northern margin of Sichuan Basin, South China. *Int. Geol. Rev.* **2022**, *64* (15), 2166−2185.

(34) Liu, Y.; Qiu, N.; Xie, Z.; Yao, Q.; Zhu, C. Overpressure compartments in the central paleo-uplift, Sichuan Basin, southwest China. *AAPG Bull.* **2016**, *100* (5), 867−888.

(35) Nie, H.; Jin, Z.; Sun, C.; He, Z.; Liu, G.; Liu, Q. Organic Matter Types of the Wufeng and Longmaxi Formations in the Sichuan Basin, South China: Implications for the Formation of Organic Matter Pores. *Energy Fuels* **2019**, *33* (9), 8076−8100.

(36) Zhang, Y.; He, Z.; Lu, S.; Jiang, S.; Xiao, D.; Long, S.; Gao, B.; Du, W.; Zhao, J.; Chen, G.; Li, Y. Characteristics of microorganisms and origin of organic matter in Wufeng Formation and Longmaxi Formation in Sichuan Basin, South China. *Mar. Pet. Geol.* **2020**, *111*, 363−374.

(37) Teichmueller, M.; Leythaeuser, D.; Ruellkotter, J. Organic petrology of source rocks, history and state of the art. *Org. Geochem.* **1986**, *10* (1−3), 581−599.

(38) Liu, D.; Xiao, X.; Tian, H.; Min, Y.; Zhou, Q.; Cheng, P.; Shen, J. Sample maturation calculated using Raman spectroscopic parameters for solid organics: Methodology and geological applications. *Chin. Sci. Bull.* **2013**, *58* (11), 1285−1298.

(39) Liu, J.; Li, S.; Wang, Y. Molecular Dynamics Simulation of Diffusion Behavior of CH4, CO2, and N2 in Mid-Rank Coal Vitrinite. *Energies* **2019**, *12* (19), 3744.

(40) Lünsdorf, N. K.; Lünsdorf, J. O. Evaluating Raman spectra of carbonaceous matter by automated, iterative curve-fitting. *Int. J. Coal Geol.* **2016**, *160−161*, 51−62.

(41) Wilkins, R. W. T.; Sherwood, N.; Li, Z. RaMM (Raman maturity method) study of samples used in an interlaboratory exercise on a standard test method for determination of vitrinite reflectance on dispersed organic matter in rocks. *Mar. Pet. Geol.* **2018**, *91*, 236−250.

(42) Xiao, X.; Zhou, Q.; Cheng, P.; Sun, J.; Liu, D.; Tian, H. Thermal maturation as revealed by micro-Raman spectroscopy of mineral-organic aggregation (MOA) in marine shales with high and over maturities. *Sci. China: Earth Sci.* **2020**, *63* (10), 1540−1552.

(43) Wilkins, R. W. T.; Boudou, R.; Sherwood, N.; Xiao, X. Thermal maturity evaluation from inertinites by Raman spectroscopy: The 'RaMM' technique. *Int. J. Coal Geol.* **2014**, *128−129*, 143−152.

(44) Sauerer, B.; Craddock, P. R.; AlJohani, M. D.; Alsamadony, K. L.; Abdallah, W. Fast and accurate shale maturity determination by Raman spectroscopy measurement with minimal sample preparation. *Int. J. Coal Geol.* **2017**, *173*, 150−157.

(45) Solum, M. S.; Sarofim, A. F.; Pugmire, R. J.; Fletcher, T. H.; Zhang, H. 13 C NMR Analysis of Soot Produced from Model Compounds and a Coal. *Energy Fuels* **2001**, *15* (4), 961−971.

(46) Liu, J.; Luo, L.; Ma, J.; Zhang, H.; Jiang, X. Chemical Properties of Superfine Pulverized Coal Particles. 3. Nuclear Magnetic Resonance Analysis of Carbon Structural Features. *Energy Fuels* **2016**, *30* (8), 6321−6329.

(47) Kelemen, S. R.; Freund, H.; Gorbaty, M. L.; Kwiatek, P. J. Thermal Chemistry of Nitrogen in Kerogen and Low-Rank Coal. *Energy Fuels* **1999**, *13* (2), 529−538.

(48) Kelemen, S. R.; Afeworki, M.; Gorbaty, M. L.; Sansone, M.; Kwiatek, P. J.; Walters, C. C.; Freund, H.; Siskin, M.; Bence, A. E.; Curry, D. J.; Solum, M.; Pugmire, R. J.; Vandenbroucke, M.; Leblond, M.; Behar, F. Direct Characterization of Kerogen by X-ray and Solid-State13 C Nuclear Magnetic Resonance Methods. *Energy Fuels* **2007**, *21* (3), 1548−1561.

(49) Cui, X.; Yan, H.; Zhao, P.; Yang, Y.; Xie, Y. Modeling of molecular and properties of anthracite base on structural accuracy identification methods. *J. Mol. Struct.* **2019**, *1183*, 313−323.

(50) Hou, D.; Qiu, X.; Gong, F.; Dejam, M.; Nasrabadi, H. Characterization of kerogen molecular structure and its effect on methane adsorption behavior: A comparative study on outcrop and core samples from Longmaxi shale. *Chem. Eng. J.* **2023**, *466*, 143293.